PROTO-I AXIAL-FOCUSING EXPERIMENTS

D. J. Johnson, R. J. Leeper, W. A. Stygar, and S. A. Slutz
Sandia National Laboratories, Albuquerque, NM 87185

SAND--83-0610C
DE84 000458

The time-integrated axial (z) focus of the 4.5-cm-radius Proto I (1.5 MV, 500 kA) radial proton diode is presently limited to ~3 mm FWHM. This result is obtained with current neutralized beam transport in a gas cell with 6 Torr argon. If the vertical local divergence were the same (1° or less) as the horizotal divergence, the local divergence alone would produce a 1.5 mm FWHM focus. The axial focal size is evidently limited by time-dependent effects. These are studied by observing the beam incident upon various targets with two time-resolved pinhole cameras. The first camera observes Rutherford-scattered protons from gold targets with an array of 11 silicon PIN detectors. The second camera observes K_α -florescence from aluminum targets with 4 independently-gated microchannel plates imaging tubes.

Introduction

The final focus spot size of the ion beam generated by a radial applied B-field ion diode depends upon a numbe: of factors. The 0.9° local and 0.7° global divergence together with canonical angular momentum account for the observed total horizontal (r,θ) beam spread of 1.6°. However, in the vertical (Z) direction other systematic time-dependent effects are also important and increase the beam spread to 2°. Here the focus is dependent upon self-magnetic field bending during beam generation and transport, movement of the electric equipotential surfaces during the pulse due to diamagnetic electron flow or electron pile up, and self-magnetic field induced astigmatism associated with nonuniform current neutralization in the gas cell and ion emission across the face of the anode. The relative importance of these effects upon the axial focus is presented in this paper for two different diodes.

Apparatus

Data were acquired with the 1 TW Proto I pulse generator using the 4.5 cm and 10 cm radius diodes shown in Figs. 1 and 2. Typical electrical characteristics of the 4.5 cm diode are shown in Fig. 3. The 10 cm diode was operated at ~30% lower impedance.

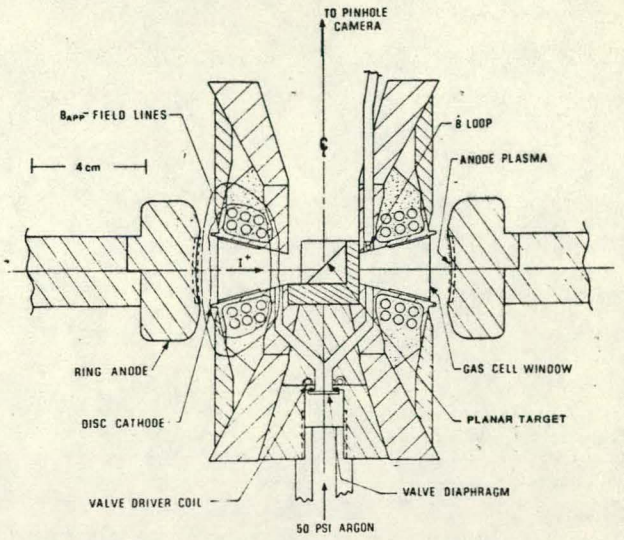

Fig. 1. Cross sectional view of the 4.5 cm radius diode.

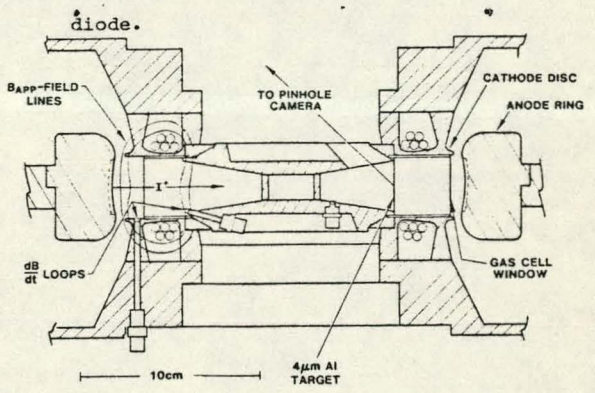

Fig. 2. Cross sectional view of the 10 cm radius diode.

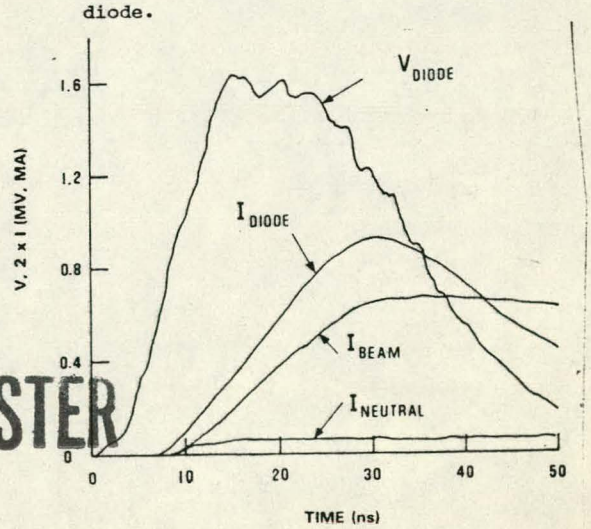

Fig. 3. Typical electrical characteristics of the 4.5 cm radius diode.

DISCLAIMER

DISCLAIMER

Both diodes have disc cathode structures with internal coils to supply the axial applied B-field (B_{app}) and aluminum anodes to confine this field. The diodes also have epoxy-filled grooved anodes as a source of anode plasma for beam generation. Protons from this plasma are accelerated toward a virtual cathode formed by electrons spiraling along the virtual B_{app}-field lines. After crossing the A-K gap the protons enter a gas cell filled with ~5 Torr argon for charge-and current-neutralized beam transport. The initial B_{app}-fields, A-K gaps, and gas cell to anode distances were 24 and 13 kG, 4.2 and 5 mm, and 5.5 and 7 mm for the small and large diode, respectively. These diodes are similar to diodes previously studied.[1,2]

The B_{app}-field configuration in the A-K gap is important in defining the virtual cathode geometry and therefore was measured experimentally for both diodes. Measurements were made with three arrays of nine large dB/dt loops mounted concentric with the anode surface in the A-K gap. Interpolation between B-flux measurements at three radii for each axial position gave the spatial position of several B-field lines. These lines are shown in Fig. 4 for the two diodes with B_o denoting the outermost field line generated by the cathode coils. The cathode structure of the 10 cm diode was designed with thick regions of stainless steel near the cathode edges to give a uniform B_{app}-field across the anode surface. This uniform field is shown in Fig. 4 for data acquired at 80 μs B-field timing. The slow negative B_{app} is primarily used to eliminate beam canonical angular momentum. It also improves the B-field curvature near the anode surface as is shown in Fig. 4 for the 4.5 cm diode. Varying the amount of slow field allows study of the relationship between B_{app}-field line curvature and focus position.

Beam diagnostics include time-integrated and time-resolved pinhole cameras to observe proton induced 1.49 keV k_α -florescence radiation (atomic excitation) from aluminum targets. The time-integrated cameras used Kodak SB-5 film filtered by 5 μm aluminum and were used on axis with the 4.5 cm diode and off axis for the 10 cm diode. The time-resolved camera uses 4 independently-gated microchannel plate (MCP) imaging tubes behind 4 individual pinholes. The sealed 18 mm dia MCP imaging tubes were coupled to 50 μm thick NElll-A scintillators. This system gave 3 ns exposures of the beam profile with 4 ns separation.

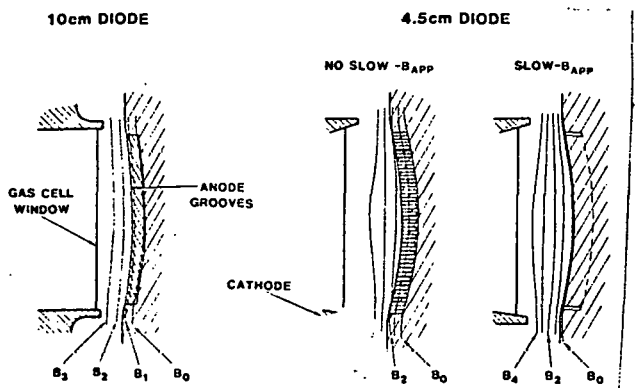

Fig. 4. Experimentally measured B_{app}-field line locations for the two diodes.

The third diagnostic observed Rutherford scattered protons from gold targets with an array of 11 silicon PIN diodes behind a pinhole camera. The diodes were mounted in a cross array to give a 2-D profile of the focused beam envelope. The diodes observed the image of an 83° sector of the beam focused upon a 2600 A planar gold target mounted at 45° to the diode center line as shown in Fig. 5. The 1 mm^2 area detectors were mounted 15 cm from the target to minimize proton time-of-flight dispersion. The pinhole was 0.25 mm diameter. Carbon ions and UV light were stopped with a 4 μm Al filter. This configuration allowed measurement of the proton current density at 7 points along the axial direction and 5 along the horizontal direction.

Discussion

The beam astigmatism has been determined for the 4.5 cm diode by a number of techniques such as measurement of the time-integrated beam profiles at various radii and positions via beam shadow edges produced by knife edges at the entrance to the gas cell. These measurements indicate that the top and bottom beam trajectories are pointed inward by 2° more than those near the midplane for circular anode curvatures. This is sufficient to broaden the focus

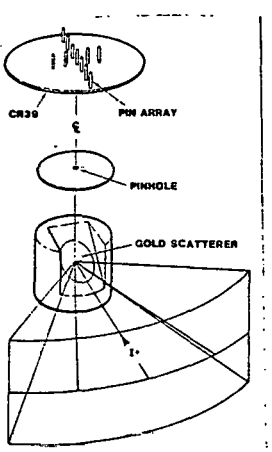

Fig. 5. Artist's conception of the PIN diode array pinhole camera system.

by ~0.5 mm and complicate diagnostics of other beam defocusing effects. The amount of astigmatism is more than that expected due to self-magnetic field bending for a beam enhanced by a factor of two near the cathode edges. This may be due to poorer current neutralization near the cathode disc where additional transverse B_{app}-flux exists or some unknown effect in the A-K gap. The details and causes of astigmatism will be left to later studies because of the subtlities of the effect.

The non-astigmatic beam focusing mechanisms can be modeled like an optical system with four simple lenses. Each beam focusing mechanism is assigned a focal length which, when combined according to the lens formula,

$$1/L_F = 1/L_A + 1/L_B + 1/L_S + 1/L_E$$

gives the beam focal position, L_F, with respect to the anode surface. These assignments allow an understanding of how the diode focuses.

The first focusing element is the anode curvature. The second is the bowing of the B_{app}-field lines with respect to the anode surface. This element has a normally negative focal length, L_B, which varies with the cathode structure and the ratio of the slow and fast B-fields used. Here we specify L_B from the curvature of the B_{app}field lines which intersects the top and bottom edges of the anode surface.

The third focusing element is due to calculated, simple self-magnetic field bending in the (r,Z) plane. This bending has focal length, L_S, specified by the peak total diode current in the A-K gap and 60 kA of non-neutralized current in the gas cell. The experimental diode focal positions with respect to the anode, L_F, were measured for the 4.5 cm radius diode with the time-integrated pinhole camera using multi-sectored conical targets and a 4.5 cm radius of curvature anode. This allowed a specification of the focal length, L_E, of the fourth element. This is the bowing of the electric field equipotentials surfaces with respect to the B_{app}-field lines. The value of L_E was found to be 18 cm when the diode was operated with and without slow B_{app}-field. The diode parameters are listed in cm in the table below.

	L_F	L_A	L_B	L_S	L_E
4.5 cm, no slow	5	4.5	-8.1	20.5	18
4.5 cm, slow	4.2	4.5	-11.5	20.5	18
10 cm, no slow	7.5	12	-560	43	36

A similar study was made for the 10 cm diode. The value of L_E was determined by two time-integrated techniques using an anode with 12 cm radius of curvature. First L_E was specified by noting that ion beamlets transmitted through a 2-D aperture array plate at 6.4 cm converged into a line array upon a brass witness cylinder at 2.5 cm radius. Secondly, the height of the beam envelope was measured at 6.4 cm diode radius with the atomic excitation pinhole camera. This measurement involved observing k_α-radiation from the rear surface of the 4 μm thick aluminum foil target shown in Fig. 2. This measurement served the dual purpose of examining beam uniformity. The reduction in beam current density at the diode midplane is 10 and 50% for experiments with and without slow B-field partially because of the positive L_B for the first beam but also because this beam used a larger A-K gap. The parameters for experiments without slow field is also shown in the table.

The small value of L_E demonstrates that an additional bending term exists which is 15% larger than self-magnetic bending. This is consistent with ~50% of non-current-neutralized ion flow in the gas cell in regions of transverse B_{app}-field. However, since ion dB/dt loops indicate 85% current neutralization in these regions effect may be occurring in the A-K gap. Reducing the gas cell radius by 1 cm caused more than a factor of two increase in magnetic bending. This supports the model of 85% current neutralization in the cell but could be caused by changes in AK physics.

The time-resolved data obtained with the MCP imaging tube and PIN camera systems are shown in Figs. 6 and 7. The MCP scans are corrected for spatial gain variations, film non-linearity, and are indicated at the time the beam strikes the target. The PIN data are not corrected for detection sensitivity or proton time of flight. The data from both systems indicate an axial and horizontal FWHM of 2.4 mm at peak proton current. A correction for the horizontal target slant angle gives a horizontal beam FWHM of 2.0 mm. The early time PIN data show a proton beam turn on delay of 2 ns with respect to the total diode current. This is consistent with the delay typically observed with the ion current dB/dt loops prior to onset of current neutralization. (See Fig. 3.) Also all of the PIN traces increase by a factor of 10 between 20 and 30 ns demonstrating little change in the focus size a[illegible] ion current increases at early time. This i[illegible]ces a constant

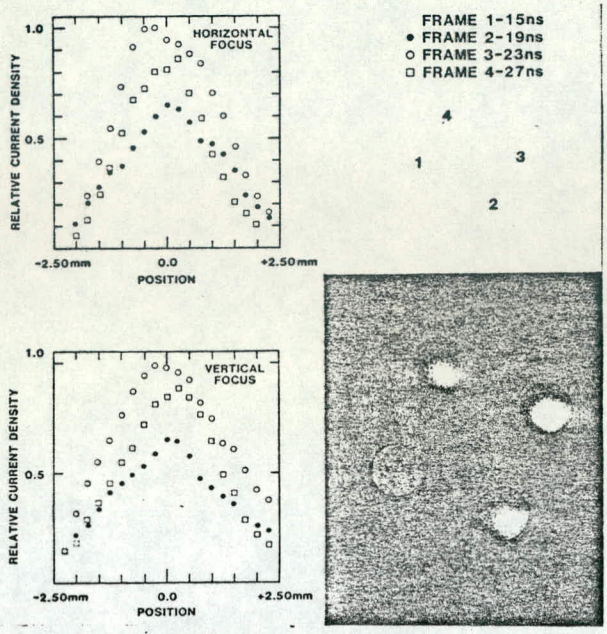

Fig. 6. Experimental data from the 4.5 cm diode acquired with the 4-frame MCP camera. The traces shown below the photos are the relative beam current densities in the horizontal and axial direction obtained from the experimental photos.

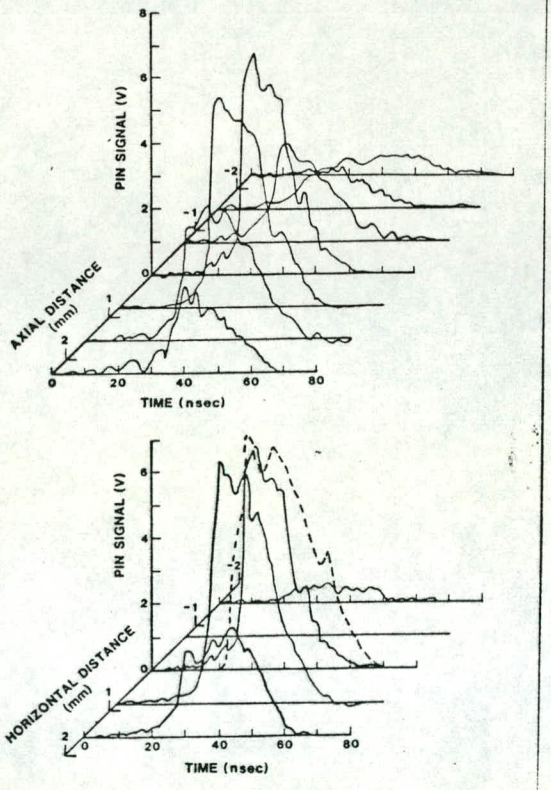

Fig. 7. Experimental signals obtained with the PIN diode array camera.

or temporally increasing L_E which compensates for L_S. This supports the conclusion of good current neutralization within the gas cell. The mechanism for this effect is not understood but fortunately does not give detrimental time-dependent defocusing. The late time PIN data show that the focus size is 2 to 3 times larger than 2.4 mm between 40 and 50 ns. This is probably due to the divergence increasing with decreasing diode impedance. In the horizontal plane the PIN data indicate a 1 mm off axis shift in the focus position. This is attributed to canonical angular momentum due to B_{app}-flux outside the anode plasma.

Conclusions

We have examined the time-resolved proton beam focus size and noted that it is 10 to 20% smaller than the time-integrated value early in time but a factor of two larger late in time due to divergence growth. Also we have noted an effect that moves the focus closer to the anode by amount about equal to self-magnetic field bending at peak current. This effect could be due to poorer current neutralization in the gas cell or distortion of equipotentials in the AK gap.

References

1. D. J. Johnson, E. J. T. Burns, A. V. Farnsworth, Jr., R. J. Leeper, J. P. Quintenz, K. W. Bieg, D. L. Fehl, J. R. Freeman, and F. C. Perry, J. Appl. Phys. 53, 4579 (1982).
2. D. J. Johnson, P. L. Dreike, S. A. Slutz, R. J. Leeper, E. J. T. Burns, J. R. Freeman, T. A. Mehlhorn, and J. P. Quintenz, J. Appl. Phys. 54, 2230 (1983).